Applied Physics Letters

Piezoelectricity and electrostriction in ferroelastic materials with polar twin boundaries and domain junctions

Cite as: Appl. Phys. Lett. **114**, 202901 (2019); https://doi.org/10.1063/1.5092523
Submitted: 11 February 2019 . Accepted: 04 May 2019 . Published Online: 20 May 2019

Guangming Lu, Suzhi Li, Xiangdong Ding, and Ekhard K. H. Salje

Piezoelectricity and electrostriction in ferroelastic materials with polar twin boundaries and domain junctions

Cite as: Appl. Phys. Lett. **114**, 202901 (2019); doi: 10.1063/1.5092523
Submitted: 11 February 2019 · Accepted: 4 May 2019 ·
Published Online: 20 May 2019

View Online Export Citation CrossMark

Guangming Lu,[1,2] Suzhi Li,[1,a)] Xiangdong Ding,[1] and Ekhard K. H. Salje[1,2,a)]

AFFILIATIONS

[1]State Key Laboratory for Mechanical Behavior of Materials, Xi'an Jiaotong University, Xi'an 710049, China
[2]Department of Earth Sciences, University of Cambridge, Cambridge CB2 3EQ, United Kingdom

[a)]Authors to whom correspondence should be addressed: lisuzhi@xjtu.edu.cn and ekhard@esc.cam.ac.uk.

ABSTRACT

Weak piezoelectricity, compared with electrostriction, occurs in twinned ferroelastic materials even when the uniform bulk material is centro-symmetric. In a simple computer simulation, polarity is exclusively generated by the flexoelectric effect. Simple twinned structures (parallel twin walls) are electrostrictive and show no piezoelectricity. Complex twinned structures break inversion symmetry by the simultaneous appearance of junctions, kinks, needle domains, etc. Such structures show weak piezoelectricity ($d \sim 10^{-4}$ pm/V) under periodic boundary conditions together with significant electrostriction. The macroscopic piezoelectric response is stronger ($d \sim 10^{-3}$ pm/V) under free boundary conditions due to the effect of relaxing surfaces.

Seemingly isotropic ceramics show unexpected macroscopic polarity in the Garten-Trolier-McKinstry scenario,[1] where some inherent polar instability is generated by the flexoelectric effect. Similar observations by Biancoli *et al.*[2] triggered extensive experimental investigations of piezoelectric materials such as quartz ceramics of different grain sizes,[3] where surprisingly strong piezoelectricity was found in agate, novaculite, and sandstone.[4] Simultaneously, electrostrictive deformation ($\sim E^2$) is commonly detected. During such studies a surprising observation was made, namely that in incommensurate phases[5] and unpoled relaxor ferroelectrics[6] the magnitudes of electrostrictive and piezoelectric effects at an applied voltage of *ca.* 10 V/mm are of similar order. Subsequent theoretical considerations and the simulations of the relevant microstructures using computer models[7] showed that similar effects were found when the polarity is completely absent in the bulk of the material and restricted to ferroelastic twin boundaries.[8] The atomistic mechanism is related to the bias polarization of the first grains, which nucleate to weakly polarize all subsequently transforming parts of the sample. The final macroscopic polarization is then correlated with the first polar nucleus or a polar twin boundary. This result is relevant to the field of domain boundary engineering[9] where domain boundary structures are constructed in specific geometrical patterns to optimize the macroscopic performance of the sample. Typical examples are polarity anomalies in twinned $SrTiO_3$ at low temperatures,[10,11] alloys,[12] and minerals.[13,14] The archetypal ferroelastic material with polarity in domain walls (but not in the bulk) is $CaTiO_3$,[15–18] which also shows piezoelectric resonances. Sluka *et al.*[19] argued that the charging of domain walls in $BaTiO_3$ is one of the main reasons for its very large piezoelectric effect.

We report in this paper that piezoelectricity occurs in simple materials without enhancing the electronic effects or dielectric anisotropies related to the geometrical pattern formation of domain walls. We found that electrostriction dominates in simple patterns (such as stripe twin patterns), while in complex patterns with many domain wall intersections, piezoelectricity and electrostriction both occur. This opens the way either to construct device materials in a statistical manner where complex domain structures promote macroscopic polarity or to predict what happens when the design faults (such as unwanted wall junctions) fundamentally modify the electric or elastic response of the material.[20,21]

The molecular dynamics simulations are based on a simple two-dimensional toy model that consisted of two atoms (A and B) carrying charges.[8] The twin structure of the ferroelastic anion sublattice A is constructed using anharmonic elastic interactions (Landau springs) while the interactions between atoms of sublattice B and between sublattices A and B are purely harmonic to exclude any additional polar instability of the bulk. The polarity of twin walls is therefore induced only by flexoelectricity caused by the change in strain gradients across twin walls and near surfaces. All model parameters are maintained from our previous study.[8] We compute the nanostructures of the twinned ferroelastic material under two different boundary conditions. The first boundary condition is periodic. The relevant simulations (using the LAMMPS code) maintain the number of particles N, temperature T, and pressure P, known as the NPT ensemble.[22] The second type of boundary condition is "open" (free boundary condition), namely, the surface atoms are specified to be stress-free (Neumann condition). In order to eliminate the surface charge effects, we add an outer layer of B atoms to the surfaces where A atoms would be the termination atoms. The charges in this layer are $1/2$ for each layer. Simultaneously, we also reduce the changes of the opposite surface layers to $1/2$. The four B atoms at the corner of the simulation box have the charge $1/4$. This means that the sample surface consists of B atoms, while charge neutrality is maintained. Strains were calculated for periodic boundary conditions using the averaged sample box dimensions (in x- and y-directions and the angle between x and y). For free boundary conditions, additional weak surface relaxations occur. We subtract these strains from the macroscopic strains for the determination of the total field induced strains.

We define two parameters to characterize the electromechanical coupling. The piezoelectric coefficients are $d_{ijk} = \frac{\partial \varepsilon_{ij}}{\partial E_k}$ ($i, j = 1, 2$ and $k = 1, 2$) at constant stress, where ε is the strain and E is the electrical field. The electrostrictive parameters are $Q_{ijkl} = \frac{\partial^2 \varepsilon_{ij}}{\partial P_k \partial P_l}$ ($i, j = 1, 2$ and $k, l = 1, 2$), where ε is the strain and P is the polarization density. The numerical values of piezoelectric coefficients are calculated by fitting ε (E) curves in order to get the experimentally preferred unit (pm/V) while the electrostrictive coefficients are obtained by fitting ε (P) curves ($cm^4/\mu C^2$ in experiment). All measures are taken at the extrema of all curves to compensate for bias strains. The calibration of the paraelastic phase with inversion symmetry showed no piezoelectric effect within a "noise level" of $\sim 10^{-5}$ pm/V.

We confirm that no piezoelectric effect exists in the untwinned, "cubic" structure under either boundary condition (Figs. S1–S3 and S9 in supplementary material). We then modeled the ferroelastic configuration with a shear angle of 2° in the bulk containing two horizontal twin boundaries with opposite polarization inside the twin boundaries [Fig. 1(a)]. This "simple twin model" has a size of 40 × 42 lattice units. Dipoles generated by the flexoelectric effect without an applied field are located inside and near the two twin walls [Fig. 1(b)]. The control parameter is the applied electric field. The field is applied along three directions separately, namely, along the x-axis (E_x), the y-axis (E_y), and at 45° to both axes (E_{xy}). The wall dipoles increase for fields parallel to the dipoles and decrease for fields antiparallel to the dipoles.

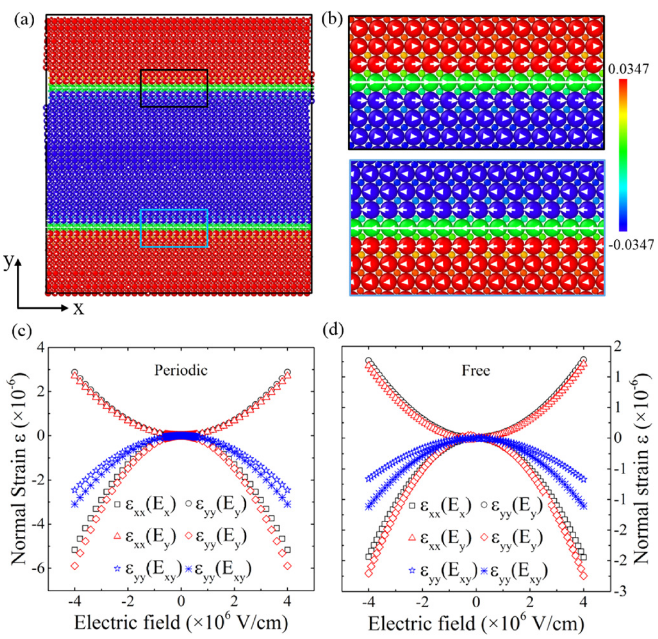

FIG. 1. The variation of strains ε_{xx} and ε_{yy} of a simple sandwich twin structure under electric fields in directions [10] (E_x), [11] (E_{xy}), and [01] (E_y). (a) Configuration of the simple twin structure and its atomic dipoles. (b) An enlarged section of the sample near the domain wall as marked in (a). The large and small spheres in (a) and (b) represent atoms of the anharmonic lattice A and the harmonic lattice B, respectively. The colors are coded according to the atomic-level shear strain. The dipole vectors between the B atoms and the center of gravity of the A atoms are shown by white arrows. The maximum dipole moment inside the domain wall is 37.6 $\mu C/cm^2$ in direction [10]. The dependence of strains ε_{xx} and ε_{yy} under E_x, E_{xy}, and E_y electric fields with (c) periodic boundary and (d) free boundary conditions. Dipole displacements are amplified by a factor of 20 for clarity.

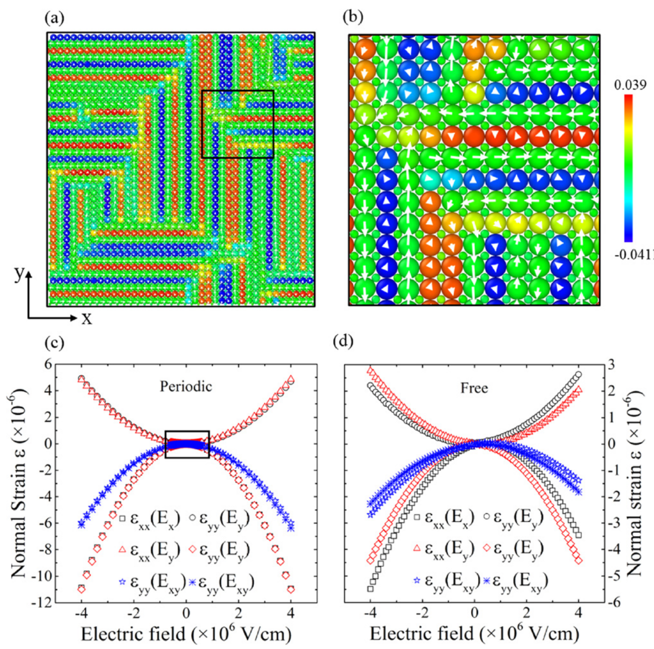

FIG. 2. The dependence of strains ε_{xx} and ε_{yy} of a complex twin structure under the electric field in directions [10, 11] and [01]. (a) Configuration of complex twin structures atomic dipoles of the entire sample. (b) An enlarged section of the junction area as marked in (a). The colors are coded according to the atomic-level shear strain. The white arrows indicate the atomic dipoles. The averaged polarization density of this junction is 0.164 $\mu C/cm^2$ in the [10] direction and −0.770 $\mu C/cm^2$ in the [01] direction. The variation of strains with the external electrical field under (c) periodic boundary and (d) free boundary conditions. Dipole displacements are amplified by a factor of 20 for clarity. The piezoelectric coefficients are $\sim 10^{-4}$ pm/V for the periodic boundary condition and $\sim 10^{-3}$ pm/V for the free boundary condition.

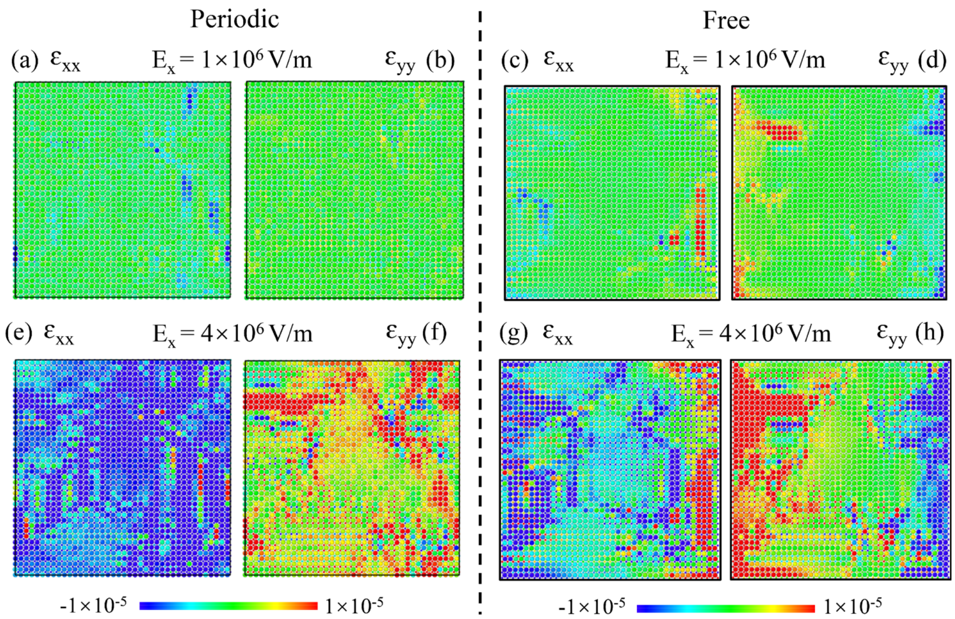

FIG. 3. Strain maps (ε_{xx}, ε_{yy}) of complex twin patterns in systems with (a)–(d) periodic boundary conditions (left panel) and (e)–(h) free boundary conditions (right panel) under different external electrical fields applied along the [10] direction. The zero-strain state corresponds to the state with $E_x = 0$.

Piezoelectricity vanishes due to the macroscopically conserved centrosymmetry of the simple structure. The strain induced by the external electric field is purely parabolic, i.e., electrostrictive [Fig. 1(c)], with $Q \sim 10^{-8}$ cm$^4/\mu$C^2. The electrostrictive coefficient is small compared with typical experimental values ($\sim 10^{-6}$ cm$^4/\mu$C^2).[23–25] Similar results were found for free boundary conditions [Fig. 1(d)] with small electrostrictive coefficients $Q \sim 10^{-9}$ cm$^4/\mu$C^2.

We then compare the strain (field induced strain, ε_{xx} and ε_{yy}) maps under the electric field with periodic and free boundary conditions (see Figs. S4–S6 in supplementary material). The initial state before applying the electric field is taken as reference. The strains for free boundaries are slightly inhomogeneous. The distribution of strain near surfaces shows virtually no supplementary strain,[26–31] which indicates that the charge compensation mechanism works very well, including the effect of the 4 corner atoms with charge $^1/_4$.

The strain patterns change drastically for complex twin patterns.[32,33] The sample (40×40 lattice units) was generated by an applied external shear in two orthogonal directions (horizontal [10] and vertical [01]), as shown in Fig. 2(a). The intersections and junctions of patterns with randomly distributed twins contain topological defects such as wall junctions and kinks inside the straight twin walls. All these geometrical elements carry local polarization [Fig. 2(b)]. The net polarization for the entire system is -5.13×10^{-4} μC/cm^2 in direction [10] and -4.75×10^{-4} μC/cm^2 in direction [01]. The piezoelectric coefficients are on the order of $d \sim 10^{-4}$ pm/V for periodic boundary condition [Fig. 2(c)] and $d \sim 10^{-3}$ pm/V for free boundary condition [Fig. 2(d)]. These values are much smaller than those found in thin two-dimensional materials, including $CrSe_2$, $CrTe_2$, CaO, CdO, ZnO, and InN, which have the in-plane piezoelectric coefficient d_{11} greater than 5 pm/V, a typical value for bulk piezoelectric materials.[34] Natvaez *et al.* drew the attention to weak surface piezoelectricity in paraelectric $BaTiO_3$,[35] although a direct quantification proved impossible. The electrostrictive coefficients Q are on the order of 10^{-8} cm$^4/\mu$C^2 for periodic boundary condition and 10^{-9} cm$^4/\mu$C^2 for free boundary condition. The asymmetric E-ε curves inside the black rectangle in Fig. 2(c) are shown in more detail in Fig. S10 of the supplementary material.

Figure 3 shows the strain maps of a complex twin structure under an electrical field E_x for both periodic and free boundary conditions. Figures 3(a)–3(d) show the strain response of topological defects (kinks, junctions, etc.). The linear field dependence of the strain relates to a weak piezoelectric effect near kinks, junctions, and dipole-dipole interactions for periodic boundary conditions. For the free boundary condition [Figs. 3(e)–3(h)], the strain response near surfaces is rather inhomogeneous, and the positive and negative strains near opposing surfaces do not compensate each other. The surface strains are on the order of 10^{-5}. The surface piezoelectricity contributes to a stronger macroscopic piezoelectric response under free boundary conditions. The strain maps for the field directions in [11] (E_{xy}) and [01] (E_y) can be found in Figs. S7 and S8 in supplementary material.

The macroscopic inversion symmetry is conserved for simple sandwich patterns and only electrostriction is observed. A high wall density additionally breaks the macroscopic inversion symmetry in complex patterns[8] and weak piezoelectricity is observed ($d \sim 10^{-4}$ pm/V). The surface piezoelectricity in complex structures under free boundary condition contributes to a stronger macroscopic piezoelectric response ($d \sim 10^{-3}$ pm/V). Compared with the simple twin structure, the electrostrictive effect for both boundary conditions is slightly stronger due to the response of dipoles residing inside junctions, kinks, and twin walls.

See the supplementary material for the complete strain maps of different systems under external electric fields such as the untwinned cubic, simple twinned and complex twinned structures.

We are grateful to NSFC (51320105014 and 51621063) and the 111 Project (No. BP 2018008) for financial support. Ekhard K. H. Salje is grateful to EPSRC (EP/P024904/1) for support. Guangming Lu was supported by a scholarship from the China Scholarship

Council. We are indebted to an anonymous referee for helpful and constructive comments.

REFERENCES

[1] L. M. Garten and S. Trolier-McKinstry, J. Appl. Phys. **117**, 094102 (2015).
[2] A. Biancoli, C. M. Fancher, J. L. Jones, and D. Damjanovic, Nat. Mater. **14**, 224 (2015).
[3] J. Aufort, O. Aktas, M. A. Carpenter, and E. K. H. Salje, Am. Miner. **100**, 1165 (2015).
[4] O. Aktas, M. A. Carpenter, and E. K. H. Salje, Appl. Phys. Lett. **103**, 142902 (2013).
[5] O. Aktas, J. R. Duclere, S. Quignon, T. Gilles, and E. K. H. Salje, Appl. Phys. Lett. **113**, 032901 (2018).
[6] O. Aktas and E. K. H. Salje, Appl. Phys. Lett. **113**, 202901 (2018).
[7] E. K. H. Salje, X. Ding, Z. Zhao, T. Lookman, and A. Saxena, Phys. Rev. B **83**, 104109 (2011).
[8] E. K. H. Salje, S. Li, M. Stengel, P. Gumbsch, and X. Ding, Phys. Rev. B **94**, 024114 (2016).
[9] E. K. H. Salje, ChemPhysChem **11**, 940 (2010).
[10] E. K. H. Salje, O. Aktas, M. A. Carpenter, V. V. Laguta, and J. F. Scott, Phys. Rev. Lett. **111**, 247603 (2013).
[11] J. F. Scott, E. K. H. Salje, and M. A. Carpenter, Phys. Rev. Lett. **109**, 187601 (2012).
[12] M. C. Gallardo, J. Manchado, F. J. Romero, J. Cerro, E. K. H. Salje, A. Planes, E. Vives, R. Romero, and M. Stipcich, Phys. Rev. B **81**, 174102 (2010).
[13] E. K. H. Salje, Phys. Chem. Miner. **14**, 181 (1987).
[14] S. A. Hayward and E. K. H. Salje, Phase Transitions **68**, 501 (1999).
[15] S. Van Aert, S. Turner, R. Delville, D. Schryvers, G. V. Tendeloo, and E. K. H. Salje, Adv. Mater. **24**, 523 (2012).
[16] L. Goncalves-Ferreira, S. A. T. Redfern, E. Artacho, and E. K. H. Salje, Phys. Rev. Lett. **101**, 097602 (2008).
[17] H. Yokota, H. Usami, R. Haumont, P. Hicher, J. Kaneshiro, E. K. H. Salje, and Y. Uesu, Phys. Rev. B **89**, 144109 (2014).
[18] E. K. H. Salje, O. Aktas, and X. Ding, "Functional topologies in (multi-)ferroics: The ferroelastic template," in *Topological Structures in Ferroic Materials*, edited by J. Seidel, Springer Series in Materials Science Vol. 228 (Springer, Basel, Switzerland, 2016), pp. 83–101.
[19] T. Sluka, A. K. Tagantsev, D. Damjanovic, M. Gureev, and N. Setter, Nat. Commun. **3**, 748 (2012).
[20] R. Hinchet, U. Khan, C. Falconi, and S. W. Kim, Mater. Today **21**, 611 (2018).
[21] E. K. Salje, S. Li, Z. Zhao, P. Gumbsch, and X. Ding, Appl. Phys. Lett. **106**, 212907 (2015).
[22] S. Plimpton, J. Comput. Phys. **117**, 1 (1995).
[23] E. K. H. Salje, M. Alexe, S. Kustov, M. C. Weber, J. Schiemer, G. F. Nataf, and J. Kreisel, Sci. Rep. **6**, 27193 (2016).
[24] F. Li, L. Jin, and R. Guo, Appl. Phys. Lett. **105**, 232903 (2014).
[25] A. L. Kholkin, E. K. Akdogan, A. Safari, P. F. Chauvy, and N. Setter, J. Appl. Phys. **89**, 8066 (2001).
[26] R. Ahluwalia, A. K. Tagantsev, P. Yudin, N. Setter, N. Ng, and D. J. Srolovitz, Phys. Rev. B **89**, 174105 (2014).
[27] A. K. Tagantsev and A. S. Yurkov, J. Appl. Phys. **112**, 044103 (2012).
[28] A. Abdollahi, F. Vásquez-Sancho, and G. Catalan, Phys. Rev. Lett. **121**, 205502 (2018).
[29] Y. M. Yue, K. Y. Xue, and T. Chen, Compos. Struct. **136**, 278 (2016).
[30] M. Stengel, Phys. Rev. B **90**, 201112 (2014).
[31] E. A. Eliseev, A. N. Morozovska, M. D. Glinchuk, and R. Blinc, Phys. Rev. B **79**, 165433 (2009).
[32] X. Ding, Z. Zhao, T. Lookman, A. Saxena, and E. K. H. Salje, Adv. Mater. **24**, 5385 (2012).
[33] E. K. H. Salje, X. Ding, Z. Zhao, and T. Lookman, Appl. Phys. Lett. **100**, 222905 (2012).
[34] M. N. Blonsky, H. L. Zhuang, A. K. Singh, and R. G. Hennig, ACS Nano **9**, 9885 (2015).
[35] J. Narvaez, S. Saremi, J. Hong, M. Stengel, and G. Catalan, Phys. Rev. Lett. **115**, 037601 (2015).